

**This is the author's final version of the contribution published as:**

Vagnon, F., Comina, C., Arato, A. Evaluation of different methods for deriving geotechnical parameters from electric and seismic streamer data (2022) Engineering Geology, 303, art. no. 106670. DOI: 10.1016/j.enggeo.2022.106670

**The publisher's version is available at:**

<https://www.sciencedirect.com/science/article/pii/S0013795222001557>

**When citing, please refer to the published version.**

This full text was downloaded from iris-AperTO: <https://iris.unito.it/>

1 **Evaluation of different methods for deriving geotechnical parameters from electric and**  
2 **seismic streamer data.**

3  
4 Vagnon Federico<sup>1\*</sup>, Comina Cesare<sup>1</sup>, Arato Alessandro<sup>2</sup>

5 <sup>1</sup> University of Torino, Department of Earth Sciences, 10125, Torino, Italy

6 federico.vagnon@unito.it; cesare.comina@unito.it

7 <sup>2</sup> Techgea S.r.L, 10137, Torino, Italy

8 arato@techgea.eu

9 \*corresponding author

10  
11 **Abstract**

12 Geotechnical parameters of linear earth structures, such as embankments and earth dams, are  
13 usually obtained from point-wise investigations through drilling or penetration tests, commonly  
14 time and cost consuming. Non-invasive geophysical investigations may be considered alternative  
15 for a preliminary screening of earth structures physical properties, given their surveying speed and  
16 their depth and length of investigation. Seismic and electrical methods can be also used, through  
17 specific correlations, for the estimation of geotechnical soil characteristics. Several methodologies  
18 have been developed over the years combining two or more geophysical techniques for the  
19 estimation of geotechnical parameters.

20 In this paper, three different methods (with theoretical, statistical, and field based approaches  
21 respectively) for geotechnical parameters estimation from integrated geophysical surveys were  
22 compared, highlighting their strongpoints and limitations also by comparison with available direct  
23 geotechnical investigations.

24 Integrated seismic and electrical data from extensive surveying performed over seven retaining  
25 structures located in Piedmont Region (NW Italy) were used to forecast their fine content and  
26 hydraulic conductivity distributions. Geophysical data were acquired using seismic and electric  
27 streamers, useful for the simultaneous execution of the surveys in motion along the earth  
28 structures. The results of this study show the effectiveness of the proposed data acquisition  
29 approach and elaboration procedures as first screening tools for earth retaining structure safety  
30 assessment. The increased capability of the theoretical method to better predict geotechnical  
31 parameters with respect to the other methodologies is also reported.

32  
33 **Article Highlights:**

- 34
- 35 • different methods for geotechnical parameters estimation from integrated seismic and  
36 electrical geophysical surveys were compared;
  - 37 • data from extensive surveying performed over seven retaining structures in Piedmont  
38 Region (NW Italy) were used to forecast fine content and hydraulic conductivity  
39 distributions;
  - 40 • strongpoints and limitations of the proposed approaches in the aim of first screening tools  
41 for earth retaining structure safety assessment are discussed.

41 **Keywords:** River embankment, Earth dam, Seismic and electric methods, Geotechnical  
42 investigations.

## 43 **1. Introduction**

44 Embankments and earth dams are engineering structures constructed for water supply, energy  
45 production or for water flow control in rivers and streams. Their stability and integrity evaluations  
46 are an important geotechnical problem for their safety assessment and the prevention from floods  
47 and dam-break related risk. Indeed, in the last five decades, these adverse phenomena have  
48 generated worldwide significant economic and human losses ([Hoyois and Sapir 2003](#)). The  
49 reported number of disasters caused by floods has dramatically increased because of climate  
50 changes and aging of most of the retaining structures.

51 Stability and integrity of these structures can be compromised by cyclic hydraulic gradients,  
52 causing seepage, internal erosion and piping especially when: i) the foundation materials are not  
53 sufficiently compacted, ii) heterogeneities are present in the embankment body or iii) the natural  
54 aging of the embankment has affected the integrity of some isolated portions. Moreover, localized  
55 invasive wildlife activities may negatively affect their hydraulic performances and their structural  
56 integrity with burrows excavated in the main embankment body or at the contact with foundation  
57 soil. All these phenomena reflect in relevant variations in the geotechnical parameters that need to  
58 be properly characterized for assessing the state of health of the structure. Moreover, in  
59 correspondance with intense rainfall events, which cause relevant hydraulic gradient variations,  
60 the timing of the characterization campaigns can be an important aspect to consider.

61 Consequently, rapid and reliable characterization tools are required for the identification of  
62 localized anomalies within the structure bodies. Conventional geotechnical methods for the  
63 characterisation involve invasive techniques such as borings (with sample collection for detailed  
64 laboratory tests) and penetration tests. These methodologies provide local detailed information of  
65 the structure layering but are affected by three main limitations: i) they provide only punctual data  
66 and are not sensitive to lateral heterogeneities, ii) they are expensive and iii) time-consuming.

67 On the other hand, non-invasive geophysical techniques allow nearly continuous determination of  
68 physical properties that can be helpful in location of anomalies and safety assessment. Given the  
69 significant linear extension of protection structures and the localized nature of weakness points,  
70 these techniques may be considered a good compromise between the surveying speed, the depth  
71 and length of investigation and reliability of the results.

72 Since the soil layering, the variation in water content and the hydraulic conditions have a great  
73 influence on the probability of global and local failure, the application of electrical resistivity  
74 methods (e.g. Electrical Resistivity Tomography, ERT) and surface wave tests (e.g. Multichannel  
75 Analysis of Surface Wave, MASW) are useful tools for linear earth structure characterization.  
76 Several applications of these methodologies can be found in literature (e.g. [Al-Fares 2014](#), [Arosio  
77 et al. 2017](#), [Camarero et al. 2019](#), [Cardarelli et al. 2014](#), [Chen et al. 2006](#), [Comina et al. 2020a](#),  
78 [Comina et al. 2020b](#), [Goff et al. 2015](#), [Hayashi et al. 2013](#), [Takahashi et al. 2014](#), [Weller et al.  
79 2014](#), [Rittgers et al. 2016](#)). In recent years, the use of mobile geoelectric and seismic systems for  
80 a preliminary characterization along river embankment has indeed risen ([Brown et al. 2011](#),  
81 [Comina et al. 2020a](#), [Comina et al. 2020b](#), [Dabas, 2011](#), [De Domenico et al. 2016](#), [Kuras et al.  
82 2007](#), [Sorensen 1996](#), [Vagnon et al. 2021](#)) due to their flexibility and increased surveying speed.

83 In complex geotechnical and hydraulic conditions, and possibly with presence of artefacts (such  
84 as metallic diaphragms or drainage pipes), a single geophysical method may lead to  
85 misinterpretations. Indeed, ERTs alone cannot distinguish whether low resistivity sectors are due  
86 to high water content or clay soil or a buried conduit. Conversely, velocity reductions evidenced  
87 by MASW could be associated both to an increase of soil fine fraction content or to an increase of  
88 the saturation degree or soil plasticity.

89 Integrated geophysical approaches, combining shear wave velocity ( $V_s$ ) and resistivity ( $R$ ), can  
90 therefore provide a more accurate description of soil type than the individual methodologies alone  
91 (Hayashi et al. 2013). In addition, several researchers have developed theoretical, statistical, or  
92 field-based methods for specific geotechnical parameters estimation (soil type, fine fraction  
93 content, porosity, hydraulic conditions) from integrated geophysical surveys (Arato et al. 2021,  
94 Brovelli and Cassiani 2010, Carcione et al. 2007, Chen et al. 2006, Cosentini and Foti 2014, Glover  
95 et al. 2000, Goff et al. 2005, Hashin and Shtrikman 1963, Hayashi et al. 2013, Takahashi et al.  
96 2014).

97 In this framework, the present paper report on extensive surveying performed over seven retaining  
98 structures located in Piedmont Region (NW Italy) by means of combined ERT and MASW  
99 surveys. Both  $R$  and  $V_s$  data were acquired over the retaining structures by means of appropriate  
100 streamers developed for these specific investigations. The geophysical data were used for detecting  
101 localized anomalies and estimating the geotechnical parameters with three different methodologies  
102 available in literature. Strongpoints and limitation of these methodologies are highlighted and  
103 discussed also in comparison with available independent geotechnical data over the same  
104 structures.

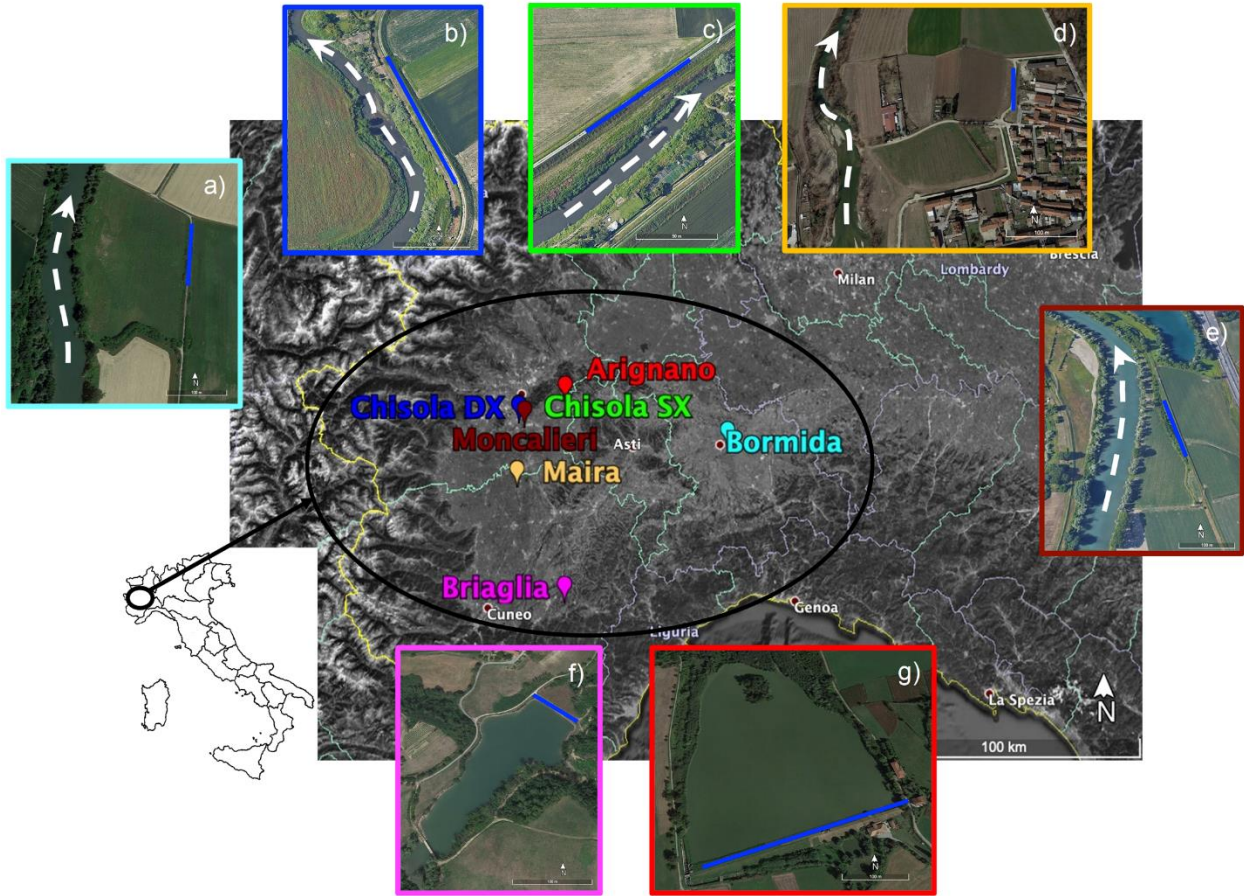
105

## 106 **2. Case studies and data acquisition**

107 Seismic and electric data were collected over seven earth retaining structures located in Piedmont  
108 Region (NW Italy): five river embankments (Bormida, Chisola DX and SX, Maira and Moncalieri)  
109 and two small earth dams (Arignano and Briaglia). Their geographical location is shown in Fig. 1  
110 and their main characteristics are summarized in Table 1 and Fig. 2.

111 These case studies were selected following three main criteria: i) availability of independent  
112 geotechnical investigations for comparing and validating geophysical results, ii) coverage of a  
113 wide range of construction materials, iii) representativeness of a wide range of structure  
114 characteristics. Regarding the last point, the analyzed sites cover different earth retaining structure  
115 typologies, characterized by different pathologies. There are two embankments characterized by  
116 known anomalies, due to animal burrows (Moncalieri) and rupture restoration works (Chisola SX),  
117 one historical embankment subjected to aging phenomena and repeatedly repaired during the time  
118 (Bormida), one embankment characterized by a potential seepage phenomenon due to the stress of  
119 several flood events (Chisola DX) and one newly built (Maira) but already showing localized  
120 instabilities. Finally, two small earth dams were also selected: a historical one with the presence  
121 of a brick channel that cross the main body (Arignano) and one built in the 1990s (Briaglia) and  
122 affected by aging phenomena.

123 Fig. 2 shows the ternary plot of the average grain size distributions for the embankment bodies and  
124 the foundation soils. These data come from point-wise geotechnical investigations performed on  
125 each analysed case study: consequently, they refer to an average soil layering and local lateral  
126 variations are neglected. As a general comment, embankment bodies are usually made by finer  
127 soils (mainly silt and clay with lower percentage of sand) compared to the foundation soils that are  
128 generally composed by fluvial deposits with high percentage of gravel and sand and potential  
129 presence of rock boulders. The differences between the properties of the main body and foundation  
130 soils in earth dams are conversely less marked, especially in the shallow portions (Fig. 2b Arignano  
131 and Briaglia markers). A short description of the tested sites is reported in the following.



132  
 133 **Figure 1.** Location of the case studies in Piedmont Region (NW Italy): a) Bormida, b) Chisola  
 134 DX, c) Chisola SX, d) Maira and e) Mocalieri embankments, f) Arignano and g) Briaglia earth  
 135 dams. Blue continuous lines and white dashed arrows respectively represent the geophysical  
 136 surveys and the river flow directions.

137  
 138 Table 1. Summary of main characteristic of the considered case studies.

Site	Retaining structure type	Average main body height [m]	Survey length [m]	Structural pathologies or potential instability warnings
Bormida	Embankment	5	90	Aging
Chisola DX	Embankment	2.5	114	Stressed by numerous flood events inducing seepage
Chisola SX	Embankment	4	110	Restored after recent flood event
Maira	Embankment	2	76	Newly built with local shallow instabilities
Moncalieri	Embankment	3	126	Presence of localized burrows from wildlife activities
Arignano	Earth dam	8	278	Aging and presence of a brick channel in the main body
Briaglia	Earth dam	11	72	Aging

140

### 141 **2.1 Bormida River embankment**

142 The right embankment of the Bormida River (44°53'51.16"N, 8°38'46.53"E, Fig. 1a), rises about  
143 7 m from the free surface of the river, and about 3 m from the surrounding floodplain. The  
144 embankment was repeatedly repaired over years after several flood events that caused local  
145 ruptures and instabilities. The soil composition of the embankment consists of silt with fine sand  
146 within the first embankment layer and fine to medium-grained sand at the interface with the  
147 foundation soil. The latter is mainly made of sand and gravel (Fig. 2).

148

### 149 **2.2 Chisola DX and SX embankments**

150 The right (DX) and left (SX) embankments of the Chisola River (44°58'43.83"N, 7°40'32.17"E,  
151 Fig. 1b and 1c respectively) have a trapezoidal shape with an average height of about 3 m above  
152 ground level, a width of about 9 m at the base and of about 4 m at the top. These embankments  
153 have been stressed by various flood events during the years, due to intense precipitations and  
154 consequent rise of water levels. In the latest event, in November 2016, a localized rupture (about  
155 40 m in length) of the left embankment (Chisola SX) occurred, and restoration works were  
156 undertaken to seal and repair the embankment. The reconstructed sector of the embankment is  
157 mainly constituted of clay and silt, while the surrounding portions and the foundation soils have a  
158 high percentage of sand (Fig. 2). The right embankment (Chisola DX) is constituted by natural  
159 silty and sandy alluvial deposits taken from the surrounding plain. This embankment was not  
160 specifically damaged by the previous floods events but given the damage of the corresponding  
161 Chisola SX the risk of seepage is considered high.

162

### 163 **2.3 Maira River embankment**

164 The Maira River embankment (44°46'13.79"N, 7°40'12.48"E, Fig. 1d) is a shallow (about 2 m)  
165 newly built embankment to protect the city of Racconigi. This embankment was constructed with  
166 selected uniform clayey material directly on the alluvial plain deposits constituted of gravelly sand  
167 (Fig. 2). The embankment experienced some landslips along the slopes, caused by the transit of  
168 heavy trucks and excavators on the crest road.

169

### 170 **2.4 Po River (Moncalieri) embankment**

171 The Po River embankment (named here Moncalieri, 44°57'50.48"N, 7°42'7.37"E, Fig. 1e) is 2 m  
172 high and was built in the early 20th century to protect the main highway from Torino towards the  
173 south. It is built with alluvial sediments (silty sands, Fig. 2) probably exploited from surrounding  
174 caves or directly from river deposits. Along this embankment, several badger burrows were  
175 detected and considered responsible of several small instabilities.

176

### 177 **2.5 Arignano dam**

178 The Arignano earth dam (45° 2'40.91"N, 7°53'26.85"E, Fig. 1f) was built at the beginning of 1800s  
179 as a water supply reservoir for agricultural purposes. The dam has a trapezoidal shape, with  
180 longitudinal extension of about 380 m, maximum height of 8 m and width, at the base, of about 60  
181 m, and at the toe of about 4 m.

182 The dam body is mostly made of silt and clay (Fig. 2) and it is founded directly on the natural  
183 alluvial soil. The peculiarity of this structure is the presence of a brick channel within the dam  
184 body, used in the past for powering the mill located downstream of the dam. This channel, 2 m

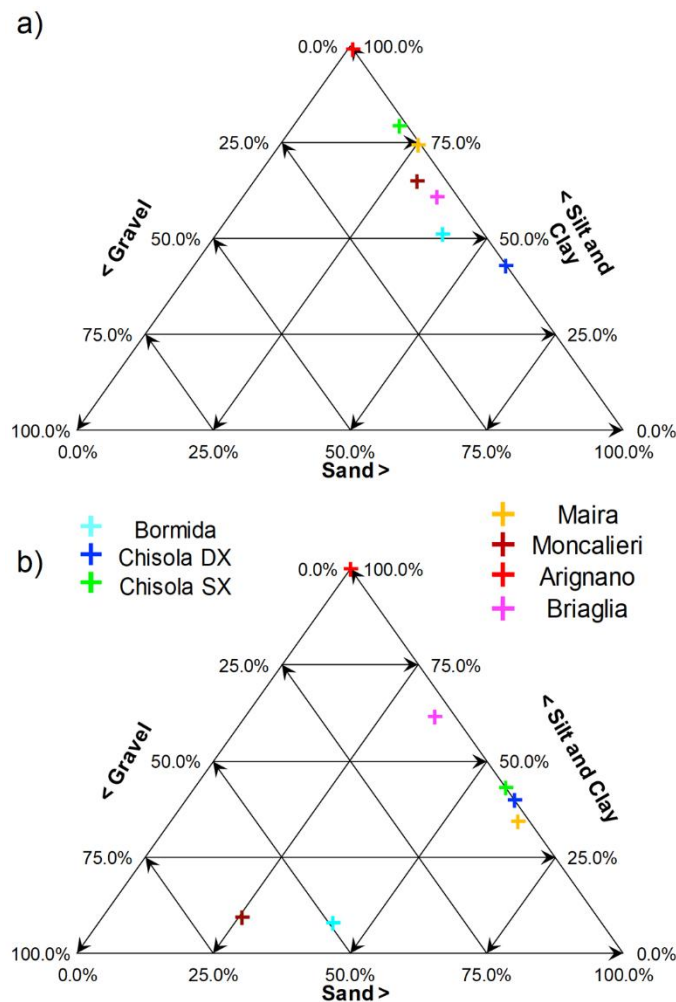
185 wide, 1.5 m tall and approximately 20 m long, has warned the authorities on the possibility of  
 186 inducing preferential seepages and local instabilities.

187

188 **2.6 Briaglia dam**

189 The Briaglia dam (44°24'10.02"N, 7°53'33.21"E, Fig. 1g) was built at the beginning of 1990s as a  
 190 water supply reservoir for agricultural purposes. It has a trapezoidal shape with a spillway and  
 191 adequate rockfill on the upstream to protect the dam from the wave flux. The dam has a total length  
 192 of about 90 m and a maximum height of about 11 m. The dam body composition varies, from the  
 193 embankment crest to the foundation soil interface, between medium-dense sandy silt to silty-  
 194 clayey sand. The foundation soil is composed of stiff clay and stiff clayey marl (Fig. 2). The dam  
 195 has been monitored in the last years to detect possible aging-related degradation of its geotechnical  
 196 performance.

197



198

199 **Figure 2.** Ternary plots of the average grain size distributions for a) the embankment bodies and  
 200 b) the foundation soils, for each analysed case study.

201

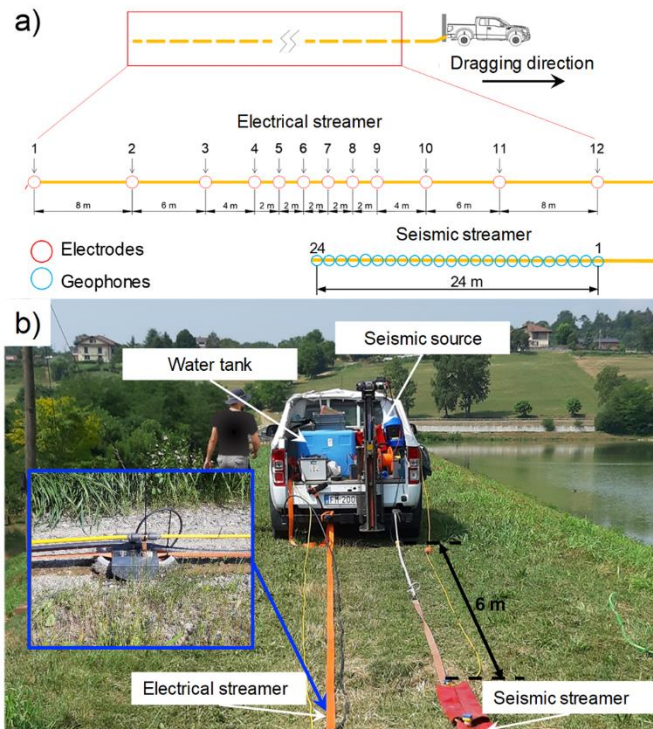
202 **2.7 Resistivity and shear wave velocity surveys**

203 The surveys over the investigated sites were performed using two different streamers dragged by  
204 a vehicle on the top of the retaining structures with data recording at 2 m steps (Fig. 3). For each  
205 step, one electric sequence and a single seismic shot were acquired. The data were referred to the  
206 respective streamer mid-points and used for integrated interpretation at the same positions. The  
207 total survey lengths for each case study are reported in Tab. 1.

208 The electric streamer consists of 12 electrodes, that can be used both as current and potential  
209 electrodes, symmetrically spaced around the streamer mid-point, with a total length of 46 m. The  
210 measurement sequence was based on Wenner-Schlumberger and Dipole-Dipole quadrupoles. The  
211 electrodes were connected to the acquisition system (Syscal-Pro, Iris Instruments,  
212 georesistivimeter), stored on the vehicle, by means of a multipolar cable. For the seismic surveys,  
213 an array of 24, 4.5 Hz vertical geophones 1 m spaced was deployed aside to the geoelectrical one  
214 and dragged by the same vehicle. A 40 kg accelerated mass was used as a seismic source and  
215 located with a 6 m offset from the first geophone. Seismograms were acquired by a DAQ-Link IV  
216 seismograph (Seismic Source) with a 0.5 ms sampling interval, -50 ms pretrig and 1.024 s total  
217 recording length.

218 Both electric and seismic acquisitions guaranteed a dense data coverage and a maximum depth of  
219 investigation (DOI) of about 10 m (actually the seismic survey DOI is deeper, see [Comina et al.](#)  
220 [2020b](#)), which is satisfactory for investigating the dam/embankment body and the first meters of  
221 foundation soil where the main instability phenomena may occur.

222 Seismic and electric data were post-processed in office: the electric data were filtered and inverted  
223 with the commercial code Res2DInv ([Loke and Barker 1996](#)) while the seismic data were analyzed  
224 with a specific procedure for the analysis of Rayleigh wave fundamental mode dispersion curves  
225 (DC). Further details on the acquisition system and data processing can be found in [Comina et al.](#)  
226 ([2020a](#), [2020b](#)).



227



228 **Figure 3.** a) Scheme of the electrical and seismic streamers adopted for the characterization. b)  
 229 Details of the seismic source and acquisition systems.

### 230 3. Methodology

231 In this section, three methods for the estimation of geotechnical parameters from integrated  
 232 geophysical data will be analysed. The methods are representative of the main approaches  
 233 developed for the characterization of earth linear structures with geophysical data: theoretical,  
 234 statistical and field-based approaches. All the three methods have been later applied to the acquired  
 235 field data in order to highlight strong points, shortcomings, and possible discrepancies between  
 236 predicted results and field evidence.

#### 237 3.1 Theoretical approach

238 Takahashi et al. (2014), and later Vagnon et al. (2021), developed an integrated method for  
 239 profiling soil permeability of river embankments by coupling seismic and electric data. The clay  
 240 content of the soil, C, (assumed as the fine soil fraction i.e. both silt and clay) can be defined from  
 241 combined geophysical data by superimposing the experimental electrical resistivity, R, and shear  
 242 wave velocity,  $V_s$ , values from field measurement to theoretical constant C curves and finding the  
 243 nearest C curve to which they can be associated. The theoretical C curves can be derived from the  
 244 theoretical  $V_s$ -porosity and R-porosity trends, defined from the Glover's model (Glover et al.  
 245 2000), the Hashin-Shtrikman upper bound model (Hashin and Shtrikman 1963) and the Voigt-  
 246 Reuss-Hill model (Mavko et al. 2009).

247 In detail, the Glover's model expresses the relationship between formation resistivity, R, and  
 248 porosity,  $\phi$ , as follows:

$$250 \frac{1}{R} = \frac{1}{R_s} (1 - \phi)^{\frac{\log(1-\phi^m)}{\log(1-\phi)}} + \frac{1}{R_f} \phi^m S_w^q \quad (1)$$

251 where  $R_s$  and  $R_f$  are the soil grains and fluid resistivities respectively, m is the cementation factor,  
 252 q is the saturation index and  $S_w$  is the saturation degree.

253 The soil grains resistivity,  $R_s$ , can be express as a function of the resistivity of the fine soil fraction  
 254 ( $R_{clay}$ ) and its content, C, by using the Hashin-Shtrikman upper bound model:

$$255 \frac{1}{R_s} = \frac{1}{R_{clay}} \left[ 1 - \frac{3(1-C)\Delta R}{\frac{3}{R_{clay}} - C\Delta R} \right] \quad (2)$$

256 with  $\Delta R$  being the difference between the electrical conductivity of the soil fine fraction,  $1/R_{clay}$ ,  
 257 and the one of the sand fraction,  $1/R_{sand}$ , i.e.  $\Delta R = \frac{1}{R_{clay}} - \frac{1}{R_{sand}}$ .

258 The theoretical relationship between  $V_s$  and porosity is evaluated by combining the Hashin-  
 259 Shtrikman lower bound and the Voigt-Reuss-Hill model as follows:

$$260 V_s = \sqrt{\frac{\left( \left( \frac{\frac{\phi}{\phi_0}}{G_{HM}+Z} + \frac{1-\phi}{\phi_0} \right)^{-1} - Z \right)}{\rho}} \quad (3)$$

261

268 with:

269

$$270 \quad Z = \frac{G_{HM}}{6} \cdot \frac{9K_{HM} + 8G_{HM}}{K_{HM} + 2G_{HM}} \quad (4)$$

$$271 \quad K_{HM} = \left[ \frac{n^2(1-\phi)^2 G_g^2}{18\pi^2(1-\nu)^2} P \right]^{\frac{1}{3}} \quad (5)$$

$$272 \quad G_{HM} = \left[ \frac{5-4\nu}{5(2-\nu)} \right] \left[ \frac{3n^2(1-\phi)^2 G_g^2}{2\pi^2(1-\nu)^2} P \right]^{\frac{1}{3}} \quad (6)$$

$$273 \quad G_g = \frac{\left[ (1-C)G_{sand} + CG_{clay} + \left( \frac{1-C}{G_{sand}} + \frac{C}{G_{clay}} \right)^{-1} \right]}{2} \quad (7)$$

274

275 and where  $\rho$  is the bulk density of the soil,  $G_{HM}$  and  $K_{HM}$  are respectively the shear and bulk moduli  
276 of the soil at the critical porosity,  $\phi_0$ , in the Hertz-Mindlin model (Mavko et al. 2009),  $n$  is the  
277 coordination number,  $P$  is the confining pressure,  $\nu$  is the Poisson's ratio of the soil,  $G_{sand}$  and  $G_{clay}$   
278 are respectively the shear moduli of sand and clay components, and  $G_g$  is the shear modulus of the  
279 soil grains.

280 These parameters can be assumed based on the wide scientific literature on this topic.

281 Once the clay content has been obtained, the porosity can be obtained by inverting Equation 1 and  
282 R-porosity and Vs-porosity relations can be obtained by using the equations above to derive the  
283 R-Vs relation. This last can be used to estimate the average grain size,  $d$ . The hydraulic  
284 conductivity can then be calculated by inserting  $d$  and the estimated porosity into the Kozeny-  
285 Carman relation (Carman 1956):

286

$$287 \quad K = 9.8 \cdot 10^6 \cdot \frac{1}{72} \cdot \frac{\phi^3}{(1-\phi)^2 \cdot (1-\ln(\phi^2))} \cdot d^2 \quad (8)$$

288

289 Many assumptions are required for the application of this formulation, particularly the value of the  
290 clay fraction resistivity,  $R_{clay}$ , has to be calibrated as a function of the specific mineralogy and  
291 cation exchange capacity of the clay present at the embankment site. Conversely the fluid  
292 resistivity,  $R_f$ , is usually available or can be easily measured independently from samples of the  
293 surrounding water. If specifically calibrated with borehole data this methodology has proven its  
294 effectiveness and reliability in profiling earth retaining structures (Takahashi et al. 2014, Vagnon  
295 et al. 2021).

296

### 297 **3.2 Statistical approach**

298 Hayashi et al. (2013) proposed a polynomial approximation for the estimation of soil parameters,  
299 such as fine fraction content (Fc), 20% average grain size (D20), blow counts from standard  
300 penetration tests ( $N_{SPT}$ ) and soil types, by using the cross-plots of shear wave velocity and  
301 resistivity.

302 They collected the results of geophysical surveys performed over 37 Japanese embankments, for  
303 a total length of 600 km and correlated them with 400 km of borings. Retaining structures soil was  
304 classified into clay, sand and gravel: further distinction was made between foundation soil and  
305 embankment body.

306 The following equation was proposed for the estimation of soil parameters:

307

308  $S_i = aV_S^2 + bV_S + c \log_{10} R^2 + d \log_{10} R + eV_S^2 \log_{10} R + fV_S \log_{10} R^2 + gV_S \log_{10} R + h$   
 309 (9)

310  
 311 where  $S_i$  is the considered soil parameter ( $F_c$ ,  $D_{20}$ ,  $N_{SPT}$  and soil type) and  $a$  to  $h$  are the polynomial  
 312 coefficients available in Hayashi et al. (2013). These latter were obtained by minimizing the  
 313 differences between each  $S_i$  and the soil parameters obtained from independent geotechnical  
 314 surveys through a least squares optimization. This formulation is therefore purely empirical, and  
 315 it is not certain how it can be applied to a broad type of soils.

316  
 317 **3.3 Field-based approach**  
 318 Chen et al. (2006) developed a seepage index ( $F$ ) for assessing potential seepage in the Laocheng  
 319 embankment (Songzi County, Hubei Province, China) by combining results from surface-wave  
 320 tests and electric resistivity measurements.  $F$  is a dimensionless index defined as:

321  
 322 
$$F = \frac{k_S}{V_S} + \frac{k_R}{R} \tag{10}$$

323  
 324 where  $k_S$  and  $k_R$  are empirical coefficients in m/s and  $\Omega m$  respectively. The index  $F$  has both a  
 325 theoretical and field-based origin. Usually, lower resistivity and shear wave velocity values are  
 326 correlated with higher moisture content. Moreover, lower shear wave velocity indicates soft soils.  
 327 Consequently, higher  $F$ -values can indicate excessive seepage or piping phenomena.

328 The values of  $k_S$  and  $k_R$  were calibrated from seismic and electric measurements and on-site  
 329 characteristics. Indeed, by superimposing  $V_S$  and  $R$  data on locations where seepage and piping  
 330 occurred, Chen et al. (2006) observed that  $F$  assumed values greater than 2. Consequently,  $k_S$  and  
 331  $k_R$  coefficients were back calculated and set respectively equal to 80 m/s and 5  $\Omega m$ . Since their  
 332 selection is not unique, the authors suggested to determine them by background values (or average  
 333 values) of shear wave velocity and resistivity through the entire dataset if no drilling data were  
 334 available. Alternatively, selection of coefficients may be done by comparing with measured  $V_S$   
 335 and  $R$  around seepage areas if such data exist.

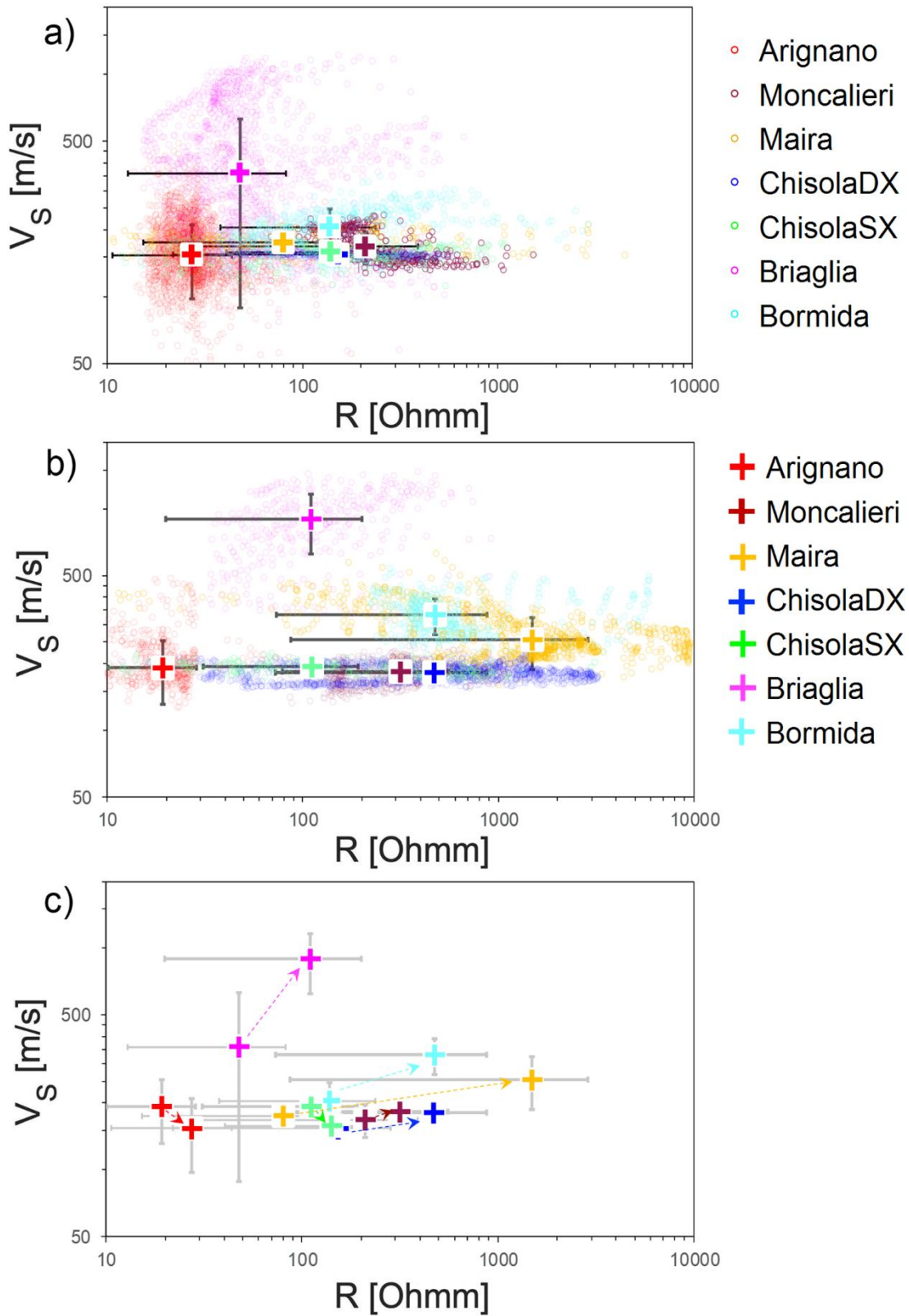
336 In this paper,  $F$  and  $k$  values were compared and the highlighted differences were analysed and  
 337 discussed with coefficients and soil parameters calibrated on each case study.

338  
 339 **4. Results**

340 Results of geophysical surveys are shown in Fig. 4. For each case study,  $V_S$ - $R$  values along the  
 341 retaining structures (circle markers) and median values (cross markers) are reported both for the  
 342 embankment body (Fig. 4a) and for the foundation soil (Fig. 4b). The shift directions between  
 343 median  $V_S$ - $R$  values of embankment body and foundation soils for each analysed structure are also  
 344 reported (Fig. 4c). For all the investigated structures the constituting soil of the embankment bodies  
 345 show lower resistivity values than foundation soil (Fig. 4c). These differences are however reduced  
 346 in some cases (i.e. Arignano, Chisola SX and Moncalieri) due to the reduced contrast among  
 347 embankment body and foundation soil. In the Arignano and Chisola SX case studies this reduced  
 348 contrast reflect in a moderate decrease in  $V_S$  from embankment body to foundation soil. In all the  
 349 other structures an increase in  $V_S$  from embankment body to foundation soil is observed. This  
 350 increase is more marked in the Briaglia dam due to the higher stiffness of the constituting  
 351 foundation soil (stiff clay).

352 At a first sight by analysing Figs 2 and 4, a good correspondence between average grain size  
 353 distributions and median  $V_S$ - $R$  values can be deduced. Generally, by increasing the sand and gravel

354 content of both embankment body and foundation soil, both resistivity and seismic velocity values  
355 increase. Indeed the evidenced shifts to higher R values from embankment body to foundation  
356 soils (Fig. 4c) is reflected in an increase in sand and gravel content (Fig. 2 a to b). Moreover, the  
357 magnitude of the resistivity shift appears proportional to the contrast between the embankment  
358 body and foundation soils.  
359



360  
 361  
 362

**Figure 4.** Distribution of the measured electrical resistivity ( $R$ ) and shear wave velocity ( $V_S$ ) values (coloured circles) in a) embankment bodies and b) foundation soils, for each analysed case

363 study. Cross markers represent the median values of the distributions, solid lines the corresponding  
364 standard deviation error bars. In a) blue cross marker (Chisola SX embankment) is partially hidden  
365 behind green cross marker (Chisola DX embankment) due to their similar properties. c) Shift  
366 directions (indicated with arrows) between median  $V_S$ -R values of embankment body and  
367 foundation soils for each analysed case study.

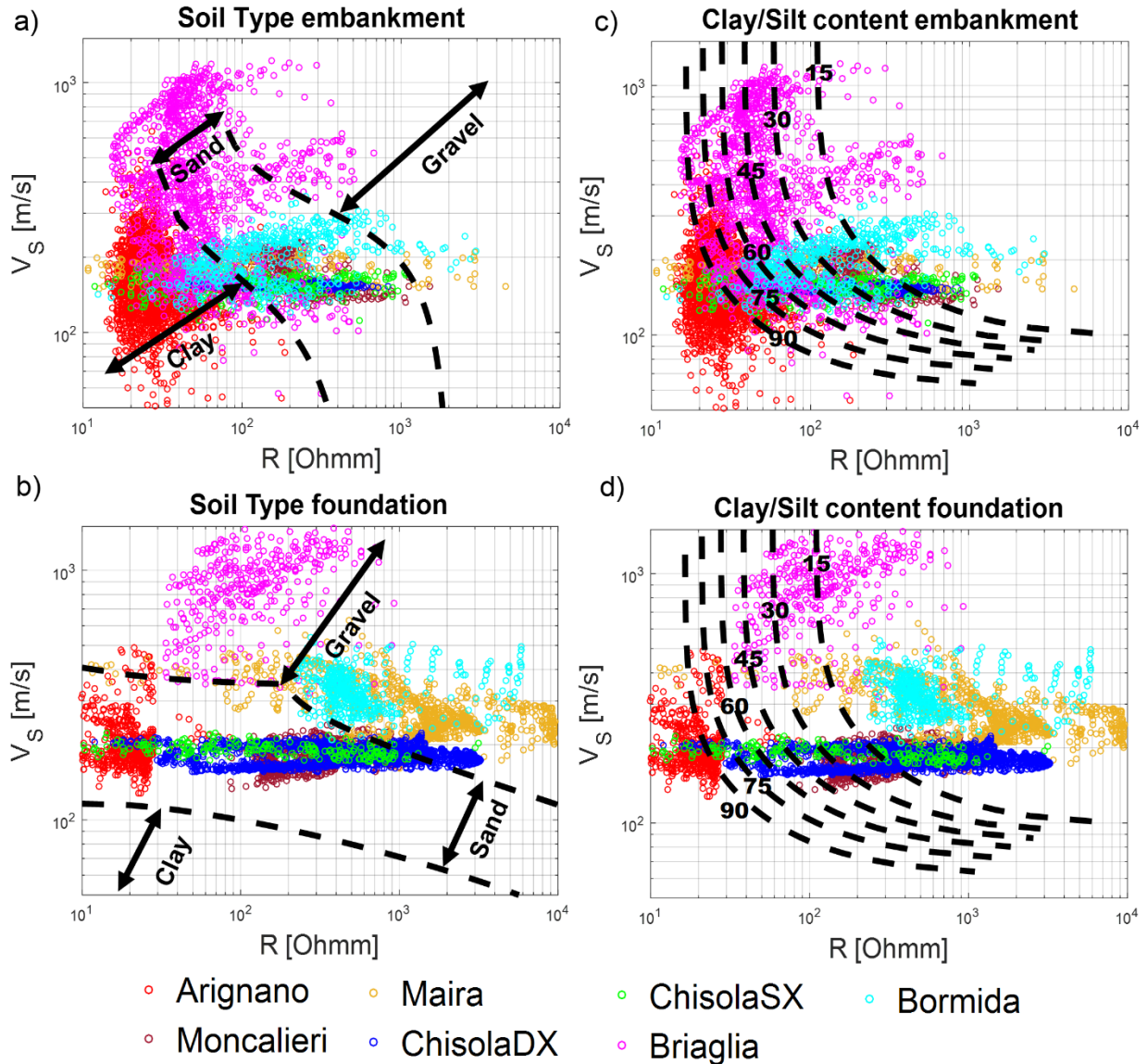
368

#### 369 **4.1 Soil Type identification**

370 Theoretical and statistical approaches allow the determination of the soil type. Soil type  
371 determination from geophysical data was therefore attempted in the investigated sites with these  
372 two methodologies (Fig. 5). With the statistical approach the soil is discretised in three classes:  
373 clay, sand and gravel with  $S_i$  values (Equation 9) ranging from 1 (clay) to 3 (gravel). In Figure 5a  
374 and 5b, the bounds between clay, sand and gravel, defined by the two black dashed lines, are  
375 reported. They were drawn by assuming Equation 9 respectively equal to 1.5 (boundary between  
376 clay and sand) and 2.5 (boundary between sand and gravel). Analogously, theoretical fine content  
377 fraction (C) curves (Figures 5c and 5d) were drawn following the methodology described in  
378 Section 3.1, assuming the clay resistivity,  $R_{clay}$ , as the minimum measured resistivity value for the  
379 given dataset and the fluid resistivity,  $R_f$ , on the basis of apriori information. The fine content  
380 fraction (C) doesn't provide by itself a clear identification of the soil type: however, many  
381 classifications available in scientific literature, are based (among other geotechnical parameters)  
382 on this parameter. As an example the standard UNI EN ISO 14688-1:2018 (CEN 2018) identifies  
383 the fine content equals to 35% as the boundary between clayey sand and silt. From 35% up to  
384 100%, the soil is classified into soft silt, soft clay, stiff clay and organic clay. The recommended  
385 soil for embankment construction falls into this group. By decreasing the fine content, clayey and  
386 silty sand, fine sand and gravel can be identified.

387 Cross-plots of R and  $V_S$  superimposed on the above defined limiting curves show that for both the  
388 analysed approaches, R- $V_S$  values for embankment body (Figures 5a and 5c) mainly fall into the  
389 sand-clay domain. Conversely, foundation soils (Figures 5b and 5d) are classified as sand and  
390 gravel. The statistical approach tends to partially overestimate the soil type granulometry  
391 especially in foundation soils (Figures 5b and 5d) compared to the theoretical one. As an example,  
392 the foundation soil of Arignano earth dam, that is totally constituted of clay (Figure 2), was  
393 predicted to be sand. Similarly, constituting soil of Briaglia earth dam foundation was predicted to  
394 be gravel instead of clayey sand.

395



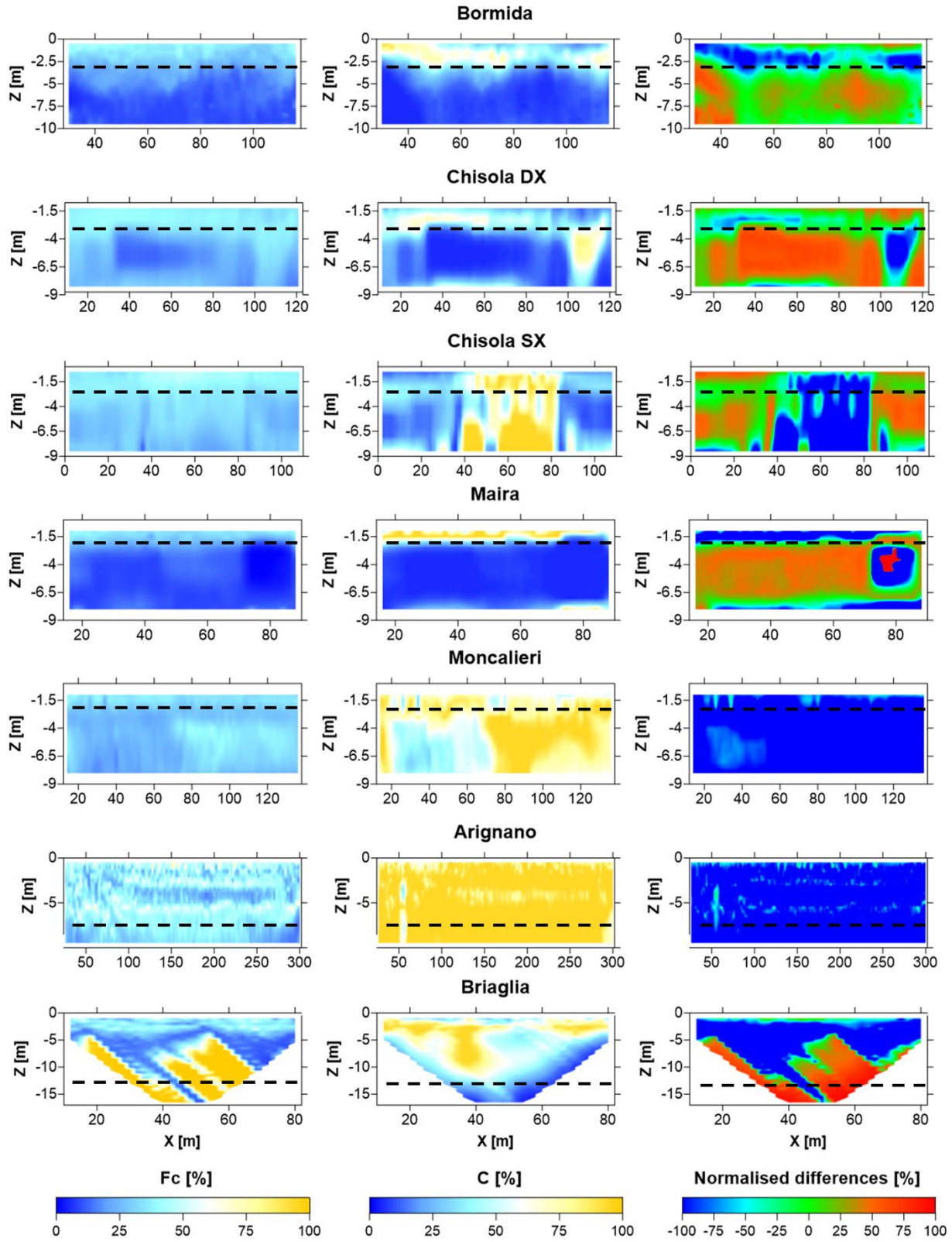
396  
 397 **Figure 5.** Soil classification as a function of shear wave velocity ( $V_S$ ) and electrical resistivity ( $R$ )  
 398 values based on a-b) Hayashi et al.(2013) approach and c-d) theoretical approach (Takahashi et  
 399 al., 2014; Vagnon et al., 2021) for embankment bodies and foundation soils . In all the plots both  
 400 the limits among different soil types from the proposed formulations (black dashed lines) and the  
 401 experimental data measured in each test sites (colored circles) are reported.  
 402

403 In order to quantitatively evaluate the differences between the two methods and evaluate the  
 404 reliability in forecasting soil characteristics, the distributions of the fine fraction contents  $F_c$  and  
 405  $C$  derived by the statistical and theoretical methods, respectively, were evaluated along the  
 406 longitudinal sections of each case study (Fig. 6). Normalised differences, defined as the ratio of  
 407 the  $F_c$ - $C$  difference to  $F_c$ , were also evaluated.

408 The two methods provide analogous results when the constituting soil is coarser and the percentage  
 409 of sand and gravel is significant (Chisola SX, Chisola DX and Bormida embankment bodies and  
 410 Maira and Bormida foundations, see also Fig. 2). Conversely, in embankments mainly constituted  
 411 by clays and silts, the statistical approach generally underestimates the fine content. For instance,

412 analysing the data from the Arignano earth dam,  $F_c$  reaches values up to 60-70%, significantly  
413 smaller than those obtained by average grain size distributions (Fig. 2). The same considerations  
414 can be made for Moncalieri and Maira embankments where fine fraction reaches 75%: barring the  
415 first meter depth where the presence of road surfacing, with coarser soil, is well identified, the  
416 clayey and silty bodies are not satisfactorily recognized by this methodology. Moreover, the  
417 method is not sensitive to sharp soil variations. By focusing on Chisola SX embankment, the  
418 statistical approach forecasts a uniform  $F_c$  distribution, which is not representative of the real  
419 setting of the embankment since the soil in correspondence of the rebuilt sector (between 40 to 80  
420 m) is more clayey than the surrounding original embankment body.  
421 Conversely, the theoretical approach is more versatile and faithfully forecasts the observed soil  
422 distributions. Sharp variations, both vertically, between embankment body and foundations and  
423 longitudinally, within the main bodies, are satisfactorily reproduced. Moreover, there is a general  
424 better correspondence among the observed  $C$  values and the ones expected on the basis of the  
425 geotechnical surveys.  
426 The predicting capability of the two previous approaches was quantitatively evaluated by  
427 comparing the predicted  $F_c$  and  $C$  results with available grain size distributions performed on  
428 borehole logs. Results are listed in Table 2. Local investigations confirm that the forecasting  
429 capability of the statistical approach is effective when the constitutive soil is coarser (such as  
430 within the main body of Bormida embankment). For clayey and silty soils, the statistical approach  
431 generally underestimates the fine fraction content up to 70%, less than what observed in borehole  
432 logs. Conversely, the theoretical approach has a higher predicting capability, independently by the  
433 overall soil characteristics of the retaining structure with average differences of 15% with respect  
434 to borehole logs.  
435





436  
437  
438  
439

**Figure 6.** Distributions of fine fraction contents  $F_c$  and  $C$  derived by the statistical and theoretical methods and their respective normalised differences for each analysed case study. In each plot black dashed lines identify the transition from the embankment body to foundation soil.

440  
441  
442  
443

**Table 2.** Comparison between fine fraction contents Fc and C derived by the statistical and theoretical methods and available grain size distribution from samples obtained in borehole logs at each test site.

	X [m]	Z [m]	Fc (<0.075m) from boreholes [%]	Fc from statistical method (Hayashi et al. 2013) [%]	Difference [%]	C from theoretical method (Takahashi et al. 2014, Vagnon et al. 2021) [%]	Difference [%]	
Bormida	48	4.8 - 5	87.6	20.95	76.08	25.00	71.46	
		7 - 7.2	11.72	10.75	8.27	10.50	10.41	
		8 - 8.2	9.72	9.72	0.02	10.00	-2.88	
		9 - 9.3	2.21	9.40	-325.20	10.00	-352.49	
Chisola SX	60	1	85.9	45.44	47.11	87.00	-1.28	
		70	1	86.3	42.90	50.29	95.00	-10.08
		84	1	54.3	40.34	25.71	57.00	-4.97
Maira	14	1	77.41	24.86	67.89	7.33	90.53	
		45	1	73.19	35.23	51.87	76.50	-4.52
		90	1	72.61	42.08	42.05	71.67	1.30
Briaglia	50	3 - 3.5	68	17.50	74.27	56.50	16.91	
		15.5 - 16	65	10.65	83.61	43.00	33.85	
Arignano	85	3.5 - 4	91.64	39.13	57.30	93.25	-1.76	
		6.5 - 7	86.51	35.49	58.97	95.00	-9.81	
	283	3.5 - 4	88.07	35.03	60.23	93.00	-5.60	
		6.5 - 7	90.52	44.90	50.40	95.00	-4.95	

444  
445  
446  
447  
448  
449  
450  
451  
452  
453  
454  
455  
456  
457  
458  
459  
460

#### 4.2 Seepage index and hydraulic conductivity estimation

In Fig. 7 the seepage index, F, and hydraulic conductivity, K, distributions for each case study are shown. F and K are intimately linked each other since they provide information on embankment hydraulic conditions and possible sectors prone to piping and seepage phenomena.

As suggested by Chen et al. (2006), the empirical coefficients  $k_S$  and  $k_R$  depend on the overall geophysical and geotechnical conditions and they may in turn be calibrated on  $V_S$  and R distributions. In this study, since no evidence of seepage phenomena were previously detected,  $k_S$  and  $k_R$  were evaluated on the basis of the minimum  $V_S$  and R values observed in the surveys.

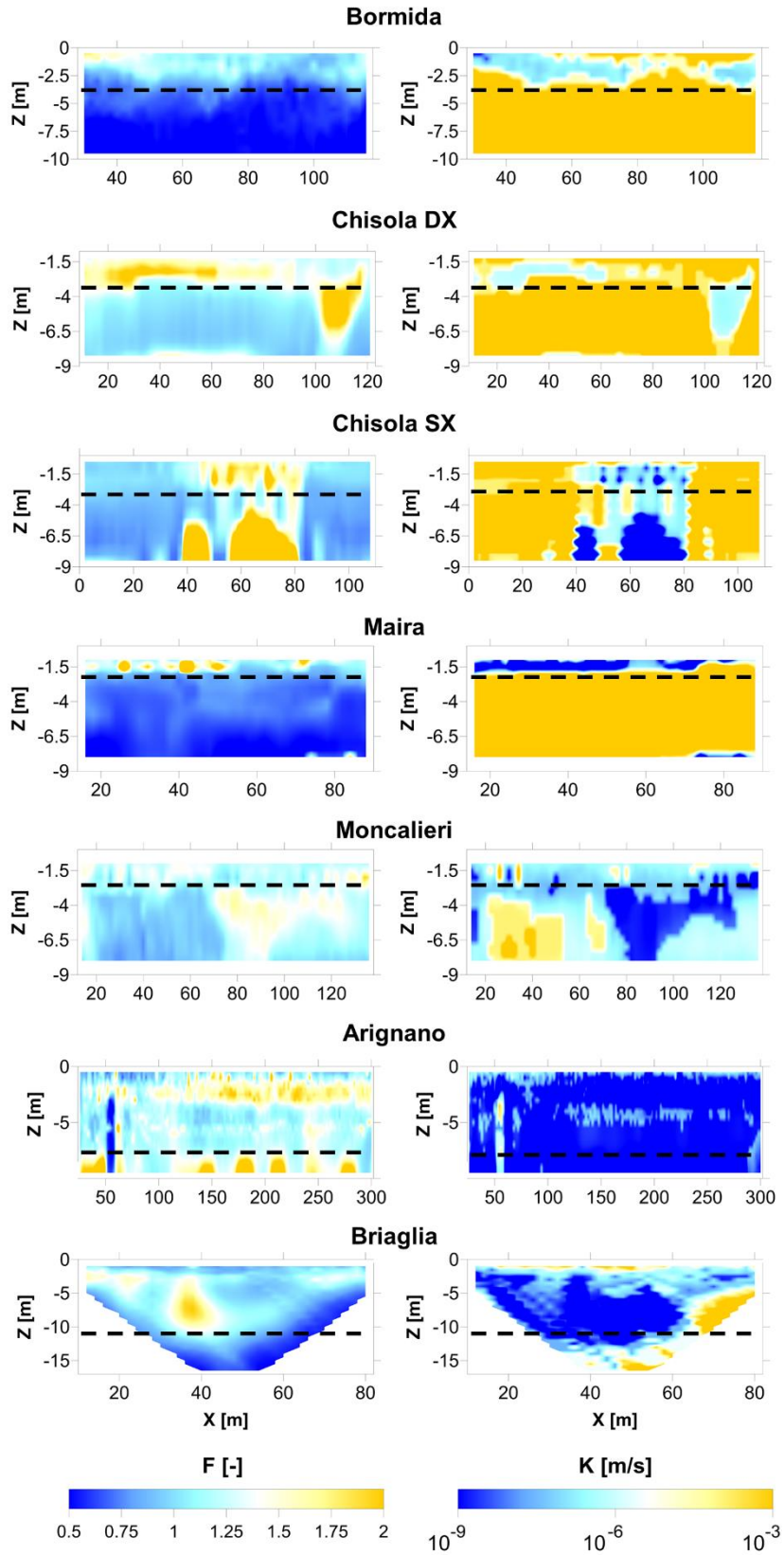
The values estimated for  $k_S$  and  $k_R$  in each test site are reported in Table 3.

The left column of Fig. 7 shows portions of the embankments with forecasted F values higher than 2 (yellow colour). In these portions there are no matches with previous geotechnical investigations of potential seepage phenomena. However, some of the reported high F values are located at the interface between embankment body and foundation (e.g Moncalieri, Maira, Chisola DX and Bormida), therefore from a theoretical point of view, their susceptibility to seepage and piping may be considered moderate to high. Conversely, Chisola SX embankment exhibits high F values ( $F > 2$ ) in correspondence of the restored portion of the levee. In this sector, compacted clays were

461 used as construction material. Seepage susceptibility may be expected at the interface between  
462 natural and restored soil but hopefully not within the latter. Therefore in this situation the field-  
463 based approach fails in identifying a strong variation in material properties attributing the R and  
464 Vs variations to potential piping effects not reflecting the real state of the embankment.

465 Contrary to the field-based approach, the theoretical approach allows the detection of sharp  
466 variations of K (right column of Fig. 7), with the main advantage of a rapid identification of the  
467 interfaces between soil with different hydraulic and geotechnical features. For instance, the  
468 presence of the brick channel along the Arignano dam (at about 50 m in longitudinal direction and  
469 at 3 m depth) is detected as a sector of high hydraulic conductivity compared to the surrounded  
470 clayey and silty soil with very low K values. This hydraulic contrast may be responsible of  
471 potential seepage and piping around the channel. The corresponding F distribution in this test site  
472 doesn't highlight this possibility (no F values higher than 2 are forecasted around the channel).  
473 Analogous observations can be extended to Chisola SX embankment where the restored soil is  
474 detected as a sector with very low K values, accordingly to the design material used during  
475 restoration works.

476  
477



479 **Figure 7.** Distributions of the seepage index F (left columns) and the hydraulic conductivity K  
 480 (right columns) for each analysed case study. In each plot black dashed lines identify the transition  
 481 from the embankment body to foundation soil. **Table 3.** List of  $k_S$  and  $k_R$  used for the evaluation  
 482 of the seepage index F for each case study.

Site	$k_S$ [m/s]	$k_R$ [ $\Omega m$ ]
Bormida	145	22
Chisola DX	172	47
Chisola SX	136	19
Maira	165	11
Moncalieri	150	79
Arignano	50	24
Briaglia	49	25

483

## 484 5. Discussions

485 From the results reported in the paper it was observed that integrated seismic and electrical  
 486 methods can be considered potentially useful tools for the characterisation of soil layering and  
 487 related geotechnical parameters since they can be linked to soils stiffness (seismic properties) and  
 488 water and clay content (electric properties), allowing for a preliminary classification as a function  
 489 of soil fraction and providing indirect correlations with other important geotechnical parameters  
 490 (e.g. hydraulic conductivity).

491 Notwithstanding this potentiality some differences were observed in the obtainable results among  
 492 the different adopted approaches, in comparison with observed borehole data, when available. The  
 493 statistical approach discrepancies between predicted and observed fine fraction values can be  
 494 related to the empirical and site-specific nature of this formulation. In fact, it was developed from  
 495 measurements performed on Japanese earth retaining structures that might be slightly different,  
 496 both in terms of geological and geotechnical features, from the embankments analysed in this  
 497 work. Consequently, a devoted calibration of the polynomial coefficients in the formulation of this  
 498 approach should be performed for optimizing the fit between estimated and observed parameters.  
 499 For this calibration however a relevant number of independent geotechnical data and several case  
 500 histories would be required.

501 On the contrary, the theoretical approach has a universal application, but it might be limited due  
 502 to numerous assumptions necessary with respect to the parameters inherent in its formulation (such  
 503 as clay and sand resistivity, interstitial water resistivity, critical porosity, saturation degree, etc.).  
 504 At the same time, this approach allows punctual calibration with geotechnical observations, even  
 505 if available in a limited number, for a detailed profiling of the retaining structure.

506 Apart from the limitations due to the soil characteristic assumptions, the main advantage of the  
 507 theoretical model is its versatility since it can be employed in different saturation and soil  
 508 conditions. Moreover, this approach also considers the confinement and the soil layering (in terms  
 509 of depth and soil density). If borehole logs are available, the theoretical approach can be calibrated  
 510 for estimating both the fine fraction content, C, and the hydraulic conductivity, K, distributions;  
 511 on the other hand, it can forecast their distributions based on average reliable parameters.

512 Particularly, the possibility of estimating the hydraulic conductivity distribution along an earth  
 513 retaining structure from geophysical data is fascinating. It must be however underlined that several  
 514 constituting properties of the clay particles, such as its mineralogy and cation exchange capacity,  
 515 are not explicitly considered in the theoretical formulation. These properties have been shown to

516 have a paramount importance in the resulting hydraulic conductivity (e.g. [Revil et al. 1999](#)). With  
517 this respect the electrical resistivity alone cannot be considered as an exhaustive parameter since  
518 electrical resistivity depends on both electrolytic conduction (fluid saturation and ionic  
519 composition) and surface conduction (in presence of clay particles or organic matter). The  
520 contributions of these two entities are not easily distinguishable in survey results from the only  
521 resistivity. Indeed, the conduction mechanisms from soil surface charge are usually mainly  
522 associated to Induced Polarisation (IP). Several applications of IP surveys to the characterization  
523 of dams and river embankments can be found in literature (e.g. [Abdulsamad et al., 2019](#); [Soueid  
524 et al., 2020](#)) exploiting this technique for a more comprehensive characterization.  
525 Nevertheless, the only electrical resistivity measurements are still often adopted as a first  
526 characterization tool since the execution of these measurements is significantly less time  
527 consuming than IP. Performing IP measurements with the same instrumentation adopted in the  
528 paper would indeed require longer current injection times, strongly increasing the surveys time. In  
529 the aims of the present work this is considered as a drawback since the study was focused on  
530 providing fast characterization tools that can be adopted as a first screening of investigated  
531 structures to be later more detailly characterized with geotechnical tests and/or with the same IP  
532 measurements particularly in correspondence of the location of the evidenced anomalies.  
533 With this respect the provided hydraulic conductivity distributions have to be considered more as  
534 a tool for identifying anomalous zones within the embankments than as an attempt to strictly  
535 quantify the hydraulic properties. In comparison with the empirical approach through the seepage  
536 index F, developed for the same aim, again the theoretical approach showed increased  
537 correspondence with available observations and a more comprehensive characterization at the  
538 different test sites reported in this paper. Particularly, at the Arignano earth dam, independent tests  
539 were performed to locally estimate the hydraulic conductivity (i.e. both variable-head hydraulic  
540 conductivity tests and laboratory oedometer tests). The results of these tests were observed to be  
541 in very good agreement with the ones from the distributions evaluated through the theoretical  
542 approach, with hydraulic conductivity values always within the same order of magnitude ([Vagnon  
543 et al. 2021](#)).

544  
545

## 546 **6. Conclusions**

547 The comparison between the analysed procedures for geotechnical parameters estimation through  
548 electric and seismic data focused on strongpoints and limitations in forecasting earth structures  
549 characteristics in comparison with previously available geotechnical investigations.

550 The electric and seismic streamer surveys and the analysed methods for geotechnical profiling  
551 represent a good compromise between quality of the estimated data, costs and surveying time. The  
552 theoretical approach, notwithstanding the limitations inherent in the calibrating parameter  
553 necessary for its formulation, proved to be more effective in geotechnical estimation of the main  
554 earth retaining structure properties. However, all the described methodologies are thought for a  
555 first screening of earth retaining structures: consequently, independent geotechnical investigations  
556 are essential for calibrating and validating obtained results. Whenever direct geotechnical data are  
557 available at some profiles along the retaining structure, geophysical models should be properly  
558 calibrated and can then be used to extend punctual direct information to the whole structure. Once  
559 relevant anomalies are identified along the investigated structures with the proposed methods more  
560 detailed geophysical investigations (e.g. Induced Polarization measurements) or direct

561 geotechnical investigations are necessary to allow a more precise definition of the geotechnical  
562 parameters of interest.

563

#### 564 **Acknowledgements**

565 This work has been partially funded by FINPIEMONTE within the POR FESR 14/20 “Poli di  
566 Innovazione - Agenda Strategica di Ricerca 2016 – Linea B” call for the project Mon.A.L.I.S.A.  
567 (313-67). Authors are gratefully to Daniele Negri for his fundamental help during acquisition  
568 surveys. Authors are also indebted with the Torino-Moncalieri AIPO division, and related  
569 personnel, for access permissions and for sharing information about the studied embankments.

570

#### 571 **References**

572 Abdulsamad, F., Revil, A., Soueid Ahmed, A., Coperey, A., Karaoulis, M., Nicaise, S., Peyras,  
573 L., 2019. Induced polarization tomography applied to the detection and the monitoring of  
574 leaks in embankments. *Eng. Geol.* 254, 89–101.

575 Al-Fares, W., 2014. Application of electrical resistivity tomography technique for characterizing  
576 leakage problem in Abu Baara earth dam, Syria. *Int. J. Geophys.* 2014.  
577 <https://doi.org/10.1155/2014/368128>

578 Arato, A., Vagnon, F., Comina, C. 2021. A new seismo-electric streamer for combined resistivity  
579 and seismic measurements along linearly extended earth structures. *Geophys. J. Int.*  
580 (accepted after minor revision)

581 Arosio, D., Munda, S., Tresoldi, G., Papini, M., Longoni, L., Zanzi, L., 2017. A customized  
582 resistivity system for monitoring saturation and seepage in earthen levees: Installation and  
583 validation. *Open Geosci.* 9, 457–467. <https://doi.org/10.1515/geo-2017-0035>

584 Bièvre, G., Lacroix, P., Oxarango, L., Goutaland, D., Monnot, G., Fargier, Y., 2017. Integration  
585 of geotechnical and geophysical techniques for the characterization of a small earth-filled  
586 canal dyke and the localization of water leakage. *J. Appl. Geophys.* 139, 1–15.  
587 <https://doi.org/10.1016/j.jappgeo.2017.02.002>

588 Brovelli, A., and Cassiani, G. 2010. A combination of the Hashin-Shtrikman bounds aimed at  
589 modelling electrical conductivity and permittivity of variably saturated porous media.  
590 *Geophys. J. Int.* 180(1), 225–237.

591 Brown, W.A., Cegon, A.B., Sheng, Z., 2011. Utilizing continuous resistivity profiling for  
592 characterization of canal seepage in El Paso, Texas, in: *Proceedings of the Symposium on  
593 the Application of Geophysics to Engineering and Environmental Problems, SAGEEP.* pp.  
594 169–178. <https://doi.org/10.4133/1.3614288>

595 Camarero, P.L., Moreira, C.A., Pereira, H.G., 2019. Analysis of the Physical Integrity of Earth  
596 Dams from Electrical Resistivity Tomography (ERT) in Brazil. *Pure Appl. Geophys.* 176,  
597 5363–5375. <https://doi.org/10.1007/s00024-019-02271-8>

- 598 Carcione, J.M., Ursin, B., Nordskog, J.I., 2007. Cross-property relations between electrical  
599 conductivity and the seismic velocity of rocks. *Geophysics* 72.  
600 <https://doi.org/10.1190/1.2762224>
- 601 Cardarelli, E., Cercato, M., De Donno, G., 2014. Characterization of an earth-filled dam through  
602 the combined use of electrical resistivity tomography, P- and SH-wave seismic tomography  
603 and surface wave data. *J. Appl. Geophys.* 106, 87–95.  
604 <https://doi.org/10.1016/j.jappgeo.2014.04.007>
- 605 Carman, P.C. 1956. *Flow of gases through porous media*. Academic Press Inc.
- 606 CEN 2018. *Geotechnical investigation and testing - Identification and classification of soil - Part*  
607 *1: Identification and description*. EN ISO 14688-1:2018.
- 608 Chen, C., Liu, J., Xia, J., Li, Z., 2006. Integrated geophysical techniques in detecting hidden  
609 dangers in river embankments. *J. Environ. Eng. Geophys.* 11, 83–94.  
610 <https://doi.org/10.2113/JEEG11.2.83>
- 611 Comina, C., Vagnon, F., Arato, A., Fantini, F., Naldi, M., 2020a. A new electric streamer for the  
612 characterization of river embankments. *Eng. Geol.* 276.  
613 <https://doi.org/10.1016/j.enggeo.2020.105770>
- 614 Comina, C., Vagnon, F., Arato, A., Antonietti, A., 2020b. Effective Vs and Vp characterization  
615 from Surface Waves streamer data along river embankments. *J. Appl. Geophys.* 183.  
616 <https://doi.org/10.1016/j.jappgeo.2020.104221>
- 617 Cosentini, R.M., Foti, S., 2014. Evaluation of porosity and degree of saturation from seismic and  
618 electrical data. *Geotechnique* 64, 278–286. <https://doi.org/10.1680/geot.13.P.075>
- 619 Dabas, M., 2008. Theory and practice of the new fast electrical imaging system ARP©, in:  
620 *Seeing the Unseen: Geophysics and Landscape Archaeology*. pp. 105–126.  
621 <https://doi.org/10.1201/9780203889558.ch5>
- 622 De Domenico, D., Garilli, G., Teramo, A., Marino, A., 2016. Application for capacitively  
623 coupled resistivity surveys in the city of messina, in: *22nd European Meeting of*  
624 *Environmental and Engineering Geophysics, Near Surface Geoscience 2016*.  
625 <https://doi.org/10.3997/2214-4609.201601963>
- 626 Glover, P.W.J., Hole, M.J., Pous, J., 2000. A modified Archie's law for two conducting phases.  
627 *Earth Planet. Sci. Lett.* 180, 369–383. [https://doi.org/10.1016/S0012-821X\(00\)00168-0](https://doi.org/10.1016/S0012-821X(00)00168-0)
- 628 Goff, D.S., Lorenzo, J.M., Hayashi, K., 2015. Resistivity and shear wave velocity as a predictive  
629 tool of sediment type in coastal levee foundation soils, in: *28th Symposium on the*  
630 *Application of Geophysics to Engineering and Environmental Problems 2015, SAGEEP*  
631 *2015*. pp. 145–154. <https://doi.org/10.4133/sageep.28-026>



- 632 Hayashi, K., Inazaki, T., Kitao, K., Kita, T., 2013. Statistical estimation of geotechnical soil  
633 parameters in terms of cross-plots of S-wave velocity and resistivity in Japanese levees, in:  
634 Society of Exploration Geophysicists International Exposition and 83rd Annual Meeting,  
635 SEG 2013: Expanding Geophysical Frontiers. pp. 1259–1263.  
636 <https://doi.org/10.1190/segam2013-0642.1>
- 637 Hashin, Z., and Shtrikman, S. (1963). “A variational approach to the theory of the elastic  
638 behaviour of multiphase materials.” *Journal of the Mechanics and Physics of Solids*, 11(2),  
639 127–140.
- 640 Hoyois, P., Guha-Sapir, D., 2003. Three decades of floods in Europe: A preliminary analysis of  
641 EMDAT data. Draft 1–15.
- 642 Kuras, O., Meldrum, P.I., Beamish, D., Ogilvy, R.D., Lala, D., 2007. Capacitive resistivity  
643 imaging with towed arrays. *J. Environ. Eng. Geophys.* 12, 267–279.  
644 <https://doi.org/10.2113/JEEG12.3.267>
- 645 Loke, M.H., Barker, R.D., 1996. Rapid least-squares inversion of apparent resistivity  
646 pseudosections by a quasi-Newton method. *Geophys. Prospect.* 44, 131–152.  
647 <https://doi.org/10.1111/j.1365-2478.1996.tb00142.x>
- 648 Mavko, G., Mukerji, T., Dvorkin, J., 2009. *The Rock Physics Handbook*, 2nd edition.  
649 <https://doi.org/10.1017/cbo9780511626753>
- 650 Revil, A., et Cathles, L.M., Permeability of shaly sands, *Water Resources Research*, 35(3), 651-  
651 662, 1999.
- 652 Rittgers J. B., A. Revil M. A. Mooney, M. Karaoulis, L. Wodajo, and C J. Hickey, 2016, Time-  
653 lapse joint inversion with automatic joint constraints, *Geophysical Journal International.*,  
654 207(3), 1401-1419,
- 655 Sørensen, K., 1996. Pulled array continuous electrical profiling. *First Break* 14, 85–90.  
656 <https://doi.org/10.4133/1.2922124>
- 657 Soueid Ahmed, A., Revil, A., Abdulsamad, F., Steck, B., Vergnialt, C., Guihard, V., 2020a.  
658 Induced polarization as a tool to non-intrusively characterize embankment hydraulic  
659 properties. *Eng. Geol.* 271.
- 660 Takahashi, T., Aizawa, T., Murata, K., Nishio, H., Consultants, S., Matsuoka, T., 2014. Soil  
661 permeability profiling on a river embankment using integrated geophysical data, in: Society  
662 of Exploration Geophysicists International Exposition and 84th Annual Meeting SEG 2014.  
663 pp. 4534–4538. <https://doi.org/10.1190/segam2014-0620.1>
- 664 Vagnon, F., Comina, C., Arato, A., Chiappone, A., Cosentini, R.M., Foti, S. 2021. Geotechnical  
665 screening of linear earth structures: electric and seismic streamers data for hydraulic

666 conductivity assessment of the Arignano earth dam. *J. of Geotech. and Geoenv. Eng.*  
667 (accepted after major revision)

668 Weller, A., Lewis, R., Canh, T., Möller, M., Scholz, B., 2014. Geotechnical and geophysical  
669 long-term monitoring at a levee of red river in vietnam. *J. Environ. Eng. Geophys.* 19, 183–  
670 192. <https://doi.org/10.2113/JEEG19.3.183>